A census of the pulsar population observed with the international LOFAR station FR606 at low frequencies (25-80 MHz)

L. Bondonneau[1], J.-M. Grießmeier[1,2], G. Theureau[1,2,3], A. V. Bilous[4], V. I. Kondratiev[5,6], other people (M. Serylak?), and more other people (PWG?)[7,8]

[1] LPC2E - Université d'Orléans / CNRS, France. e-mail: `louis.bondonneau@cnrs-orleans.fr`
[2] Station de Radioastronomie de Nançay, Observatoire de Paris - CNRS/INSU, USR 704 - Univ. Orléans, OSUC, route de Souesmes, 18330 Nançay, France
[3] Laboratoire Univers et Théories LUTh, Observatoire de Paris, CNRS/INSU, Université Paris Diderot, 5 place Jules Janssen, 92190 Meudon, France
[4] Anton Pannekoek Institute for Astronomy, University of Amsterdam, Science Park 904, 1098 XH Amsterdam, The Netherlands
[5] ASTRON, the Netherlands Institute for Radio Astronomy, Postbus 2, 7990 AA Dwingeloo, The Netherlands
[6] Astro Space Center, Lebedev Physical Institute, Russian Academy of Sciences, Profsoyuznaya Str. 84/32, Moscow 117977, Russia
[7] some place

Version of August 16, 2019

ABSTRACT

Context. The LOFAR LBA census (Bilous et al. 2019) has increased the number of pulsars with periodic pulsed radio emission detected at frequencies below 100 MHz from 69 pulsars to 83.
Aims. We aim at increasing the sample of known low-frequency radio pulsars. This will allow to probe the local Galactic pulsar population and to build a database of pulsars for further low-frequency studies, such as profile evolution with frequency, single pulses, giant pulses, spectra and turnover, dispersion measure (DM) variations, scintillation, scattering, and others.
Methods. In order to increase the sample of known low-frequency radio pulsars, we have observed 102 pulsars with known radio emission below 200 MHz and declination above $-30°$. The observations were performed with the LOw Frequency ARray (LOFAR) international station FR606 at the Nançay Radio Observatory in standalone mode, recording data from 25-80 MHz using the the Low Band Antennas (LBA).
Results. Out of our 102 targets, 64 pulsars have been detected. We confirm 10 pulsars that have been detected for the first time below 100 MHz by the LOFAR LBA census (Bilous et al. 2019), and add two more pulsars that have never been detected in this frequency range before. We provide average pulse profiles, DM values and mean flux densities (or upper limits in the case of non-detections). The comparison to previously published results allows us to identify a previously unknown spectral turnover for five pulsars, confirming the expectation that spectral turnovers are a widespread phenomenon.

Key words. Pulsar, Low Frequency

1. Introduction

1.1. Low frequency pulsar observations

Until recently, radio frequencies below 100 MHz were largely under-exploited in pulsar astronomy. The reasons for this are manifold: the interstellar medium causes high dispersion delays which lead to pulse smearing unless coherent dedispersion is used (which is computationally very expensive at such low frequencies), scattering on the inhomogeneities in the interstellar medium leads to pulse smearing (regardless of the dedispersion method), spectral turnover leads to low flux densities, the steep spectrum of the galactic background further reduces the measured signal-to-noise ratio, and the terrestrial ionosphere introduces angular shifts. Moreover, the times of arrival of pul-

sations extracted at such frequencies are highly affected by the profile frequency evolution, due to a dependency of the emission altitude in the pulsar magnetosphere on the emission frequency (radius-to-frequency-mapping, see e.g. Ruderman & Sutherland 1975; Cordes 1978).

However, these effects do not only pose problems for observations. They also constitute a treasure trove of rich and complex phenomena which can be studied with sufficiently sensitive radio telescopes. For example, following the radius-to-frequency-mapping, low frequency radio emission traces the higher altitudes in the pulsars magnetosphere. A detailed, wide-band study of low-frequency radio emission thus allows to map a large volume-fraction of the pulsar's magnetosphere. Using observations with a large fractional bandwidth and high sensitivity at low frequencies, Hassall et al. (2012) were able to put strong constraints

on the height of radio emission. Similarly, the precise measurement of the spectral turnover will allow to gain better understanding on the pulsars' radio emission mechanism, and temporal variations of the dispersion measure and of scattering can be monitored with very high precision to study the distribution of ionized plasma in the interstellar medium.

1.2. The sample of radio pulsars below 100 MHz

At the time of preparing this manuscript, 2702 pulsars are listed in the Australia Telescope National Facility (ATNF) Pulsar Catalogue[1] (Manchester et al. 2005). Out of this population, 158 slow pulsars and 48 millisecond have been detected using the LOFAR core in the frequency range 110-188 MHz (LOFAR HBA range, Bilous et al. 2016; Kondratiev et al. 2016).

At frequencies below 100 MHz, the number of pulsars detected via their periodic, pulsed radio emission is considerably lower: 40 pulsars have been detected by UTR-2 (Zakharenko et al. 2013), 44 by LWA (Dowell et al. 2013; Stovall et al. 2015), 28 non-recycled pulsars and 3 millisecond pulsars by LOFAR-LBA (Pilia et al. 2016; Kondratiev et al. 2016), and 2 millisecond pulsars by MWA (Bhat et al. 2018). Two additional pulsars have been previously reported at low significance ($<5\sigma$) by Reyes et al. (1980) and Deshpande & Radhakrishnan (1992), and three additional pulsars have been reported by Izvekova et al. (1981, without pulse profiles). Combining these publications leads to a total of 69 different pulsars. In a companion study (Bilous et al. 2019), we show results of the LOFAR core LBA census, which adds 14 pulsars not previously detected at frequencies below 100 MHz.

With this, 83 different pulsars have been detected below 100 MHz prior to this study, 82 of which are in the visible part of the sky for FR606. This represents less than 20% of the population of low-DM, non-recycled radio pulsars visible for FR606.

In view of the low number of pulsars known at frequencies below 100 MHz, we have used the French LOFAR station FR606 to conduct a systematic survey of the pulsar population below 100 MHz. Preliminary results of this survey have been already presented in Grießmeier et al. (2018). The survey is now complete, and this article details the final results.

2. Observations

Our observations have been carried out with the International LOFAR Station in Nançay, FR606, used in stand-alone mode, between 2016 and 2017. LOFAR, the Low Frequency Array, is fully described in Stappers et al. (2011) and van Haarlem et al. (2013). The international LOFAR station FR606 contains 96 LBA dipoles. These antennas can operate over the range 10-90 MHz, with a central frequency of $\sim$50 MHz and a total bandwidth of up to 80 MHz. Signals from individual LBA antennas are coherently summed, synthesizing a digital telescope. In this study, we recorded data from 25-80 MHz (i.e. a total bandwidth of 55 MHz) for pulsars with a DM < 17 pc cm^{-3} and data from

50-80 MHz (i.e. a total bandwidth of 30 MHz) for pulsars with higher DMs.

While a single LOFAR station such as FR606 only has a limited effective area, it allows for very flexible scheduling, especially for long observations or high cadence monitoring. The capability of this setup for pulsar science has already been demonstrated (Rajwade et al. 2016; Mereghetti et al. 2016, 2018; Grießmeier et al. 2018; Bondonneau et al. 2018; Tiburzi et al. 2019; Michilli et al. 2018a,b; Hermsen et al. 2018; Donner et al. 2019).

The targets for our study have been selected in the following way:

– As a basis, we considered the pulsars previously detected at low frequencies by Zakharenko et al. (2013) and Stovall et al. (2015). We have added some of the pulsars detected in the LOFAR HBA census (110 − 188 MHz Bilous et al. 2016), and some additional targets we deemed interesting.
– We kept only targets with declination $\geq -20°$. With this limit, the minimum elevation observed at Nançay Radio Observatory is of 20°, and the effective area of the telescope is $\sim$11.5% of the value for an observation at zenith. As an exception to this, we observed the bright sources B0628-28 and B1749-28 down to an elevation of 14°.
– We have discarded all targets with a dispersion measure higher than 140 pc cm^{-3}.

With these criteria, we are left with 102 targets, as detailed in Table 1 (detections) and Table A.1 (non-detections).

All pulsars were observed for a duration from one to six hours, depending on the source elevation and on constraints related to the scheduling of the radio telescope. Non-detections are based on observations of at least three hours. As a whole, the telescope time allocated to this project amounts to 294 hours (on average $\sim$3 h per target).

3. Data processing

3.1. Initial pulsar processing

The nominal observing band (26-98 MHz) was split into three band of 24 MHz each in order to spread the processing over three different computing nodes.

In order to optimize the observing time, waveform data were systematically post-processed off-line, when the radio telescope was preempted for observations in International LOFAR Telescope (ILT) mode. Our pulsar processing pipeline was based on DSPSR[2] (van Straten & Bailes 2011) which coherently dedispersed the data, folded the resulting time series at the period of the pulsar, and created sub-integrations of 10 seconds. Subsequently, observations were written out in PSRCHIVE[3] (Hotan et al. 2004) format. After this step, the data from the three recording machines were combined into a single file.

Before final analysis, each observation was refolded with an up-to-date ephemeris file when available (compiled by Smith et al. 2019). The dispersion measure (DM) values were provided by previous low frequency observations (mostly Zakharenko et al. 2013; Bilous et al. 2016).

3.2. Radio interference mitigation

We used a custom radio frequency interference (RFI) mitigation scheme in order to automatically clean the observations. A few frequency channels near the top of the band, which was frequently polluted by radio transmission, were weighted to zero to improve the mitigation process. RFI mitigation at such low frequencies is a challenge, and it is further complicated by the strongly peaked response of the LBA antennas (sensitivity maximum at ∼58 MHz, see van Haarlem et al. 2013). In the absence of any dedicated processing, strong RFI signals in the low sensitivity zone would be under-evaluated and not completely mitigated. To correct for this effect, each observation was (temporarily) flattened along the frequency axis by its (time-)average, which removes the frequency response of the instrument. A mitigation mask was then generated by running `Coast Guard`[4] (Lazarus et al. 2016) on this flattened dataset. This mask was finally applied to the initial (un-flattened) datafile.

3.3. Fine-tuning of period and DM

After RFI mitigation, we refined the pulsar's period and dispersion measure (DM) using `pdmp` (part of the software package `PSRCHIVE`). This was required to account for deviations of these values from those in the ephemeris files used during the observations (e.g. due to the limited precision of these files, or due to a variation of these parameters). Given our frequency range, this was especially critical for the DM, where a small deviation from the nominal value can smear the pulse profile considerably.

This small correction to the DM is incoherent and can in principle result in a broadening of the pulse profile, more pronounced at low frequency as $\Delta t \propto DM(f_1^{-2} - f_2^{-2})$. In our sample of detected pulsars, this incoherent dedispersion broadening ($\frac{\Delta t}{P_0}$) is less than than 2% of the pulse period, and does not affect the profile shape by more than one bin.

3.4. Classification

After visual inspection, pulsars were either classified as detections or non-detections. A pulsar was classified as a detection if (a) it had a signal-noise-ratio greater than 5, (b) was visible over a large frequency band, and was (c) detected in ≳30% of all sub-integrations.[5]

In some cases, remaining low-level RFI made the analysis ambiguous. In those cases, this RFI was manually cleaned using `pazi` (from the `PSRCHIVE` software package), and a new cycle of `pdmp` and visual inspection was required.

3.5. Flux densities of detected pulsars

Before calibration, we removed all data above 80 MHz and reduced the time resolution of the observation, increasing the length of an sub-integration to 60 seconds. This allowed to considerably decrease the processing time of the calibration.

The flux calibration software used in the paper is described in Kondratiev et al. (2016). It is based on the radiometer equation (Dicke 1946), the Hamaker beam

model (Hamaker 2006) and the `mscorpol` package by Tobia Carozzi. It calculates, for each frequency channel, the antenna response for the LBA station FR606 as a function of the pointing direction.

The fraction of flagged antennas (i.e. antennas not used during a given observation) was low (on average 2% for our observations). Due to its low impact compared to the effect of scintillation, we ignored this factor in the flux calculation.

3.6. Upper limits for non-detected pulsars

For non-detected pulsars, we defined S_{lim} as the upper limit for the mean flux density, according to the following equation (following Lorimer & Kramer 2004):

$$S_{\mathrm{lim}} = \frac{S/N(T_{\mathrm{inst}} + T_{\mathrm{sky}})}{G\sqrt{n_{\mathrm{p}}t_{\mathrm{obs}}\Delta F_{\mathrm{eff}}}} \sqrt{\frac{W/P}{1 - W/P}} \qquad (1)$$

Here,

- $S/N = 5$ is the signal-to-noise ratio limit required for a detection,
- T_{inst} is the (frequency-dependent) instrument temperature (deduced from an observation of Cassiopeia A, see Wijnholds & van Cappellen 2011),
- T_{sky} is the sky temperature interpolated from a sky map at 408 MHz (Haslam et al. 1982), scaled to our frequencies using $f^{-2.55}$ (Lawson et al. 1987),
- G is the the effective gain, which depends on the source elevation. For this, we use the Hamaker beam model (Hamaker 2006) and the `mscorpol` package,
- $n_{\mathrm{p}} = 2$ is the number of polarizations,
- t_{obs} is the duration of the observation,
- ΔF_{eff} is the effective bandwidth after RFI-cleaning,
- W and P respectively are the width of the integrated profile and the pulse period. We assume a duty-cycle of $W/P = 0.1$, which is it consistent with the profiles of the detected pulsars.

Between ∼35-75 MHz, the sky temperature T_{sky} (which is frequency- and direction-dependent) dominates over the instrument temperature T_{inst}. For example, at 60 MHz, T_{sky} is 2350 K for pointing directions away from the Galactic plane (Galactic longitude of 0°, Galactic latitude of 90°), but rises to 8500 K in the Galactic plane (Galactic longitude of 90°, Galactic latitude of 0°), and can reach up to 50000 K in the direction of the Galactic center (Galactic longitude of 0°, Galactic latitude of 0°). For comparison, $T_{\mathrm{inst}} = 140$ K at 53 MHz.

Figure 1 shows the dependence of S_{lim} on source elevation for three typical pointing directions (blue: towards the Galactic Center, with $T_{\mathrm{sky}} = 50000$ K; green: in the Galactic Plane, with $T_{\mathrm{sky}} = 8500$ K; red: outside the Galactic plane, with $T_{\mathrm{sky}} = 2350$ K). The figure is based on Equation (1), and assumes an observation duration of $t_{\mathrm{obs}} = 4$h. It shows that under optimal conditions (i.e. a high elevation source outside the Galactic plane), we can achieve an upper flux limit of ∼30 mJy, whereas it can be up to three orders of magnitude less constraining for non-ideal conditions (low elevation source in the direction of the Galactic Center). Pulsars with mean flux densities in the colored region are not detectable, regardless of their position in the sky.

In Section 4, we will use equation (1) to derive upper limits for each of our non-detections on a case-by-case basis.

---

[4] https://github.com/plazar/coast_guard/
[5] In some cases, this can exclude pulsars with a large nulling fraction, see Section 5.6.
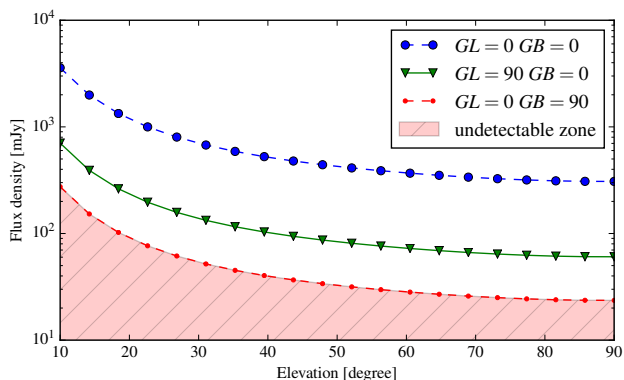
Fig. 1. Minimum observable flux density depending on the target's elevation during the observation and its location in the galaxy for a signal-to-noise ratio of 5 and an observation duration of 4h. Three different Galactic temperature and location are used. Blue: Galactic center ($gl = 0°$, $gb = 0°$, $T_{\rm sky} = 50000$ K); green: Galactic plane ($gl = 90°$, $gb = 0°$, $T_{\rm sky} = 8500$ K); red: and outside the Galactic plane ($gl = 0°$, $gb = 90°$, $T_{\rm sky} = 2350$ K). Pulsars with flux densities in the colored region are too faint, and thus undetectable for the LBA antennas of the LOFAR station FR606.

4. Results

4.1. Detection rates

Out of the 102 targets we have observed, we have successfully detected 64 pulsars (61 slow pulsars and 3 millisecond pulsars). 12 of these pulsars have either been detected in this frequency range for the first time, or have been detected in this frequency range for the first time only very recently (Bilous et al. 2019). Most of these "new" low-frequency detections overlap with the simultaneous analysis of LOFAR core data (10 out of 12, cf. Bilous et al. 2019). Compared to Bilous et al. (2019), we have detected two additional pulsars (J0108+6608 and J2022+5154) that were not in their sample and which were previously unknown at frequencies below 100 MHz.

Figure 2 compares the detected pulsars (blue and magenta points) and the non-detections (red crosses) in terms of measured DM and expected scattering delay at 60 MHz (calculated using Yao et al. 2017) relative to the pulsar period. The two small plots indicate the fraction of detected pulsars as a function of DM (lower panel) and scattering delay (right panel). As expected, pulsars become undetectable once the scatter broadening exceeds the pulsar period (central plot, and right panel).

Figure 2 also shows a correlation between high DM and high scattering timescales. This correlation is well-known, and has been described, e.g. by Bhat et al. (2004). This correlation allows us to estimate the maximum DM at which we can detect pulsars before their pulsations become undetectable due to scatter-broadening. In our case, the maximum detected DM value is ~ 57 (for B0355+54).

Of course, the DM is related to distance. We can thus estimate the maximum distance at which we can detect pulsars. For this, we look at the spatial distribution of our observations and detections. Figure 3 shows the location of our targets in the Galactic plane, with the Earth at the origin of the axes. The electron density model YMW16 from Yao et al. (2017) is represented in a gray scale. Pulsars
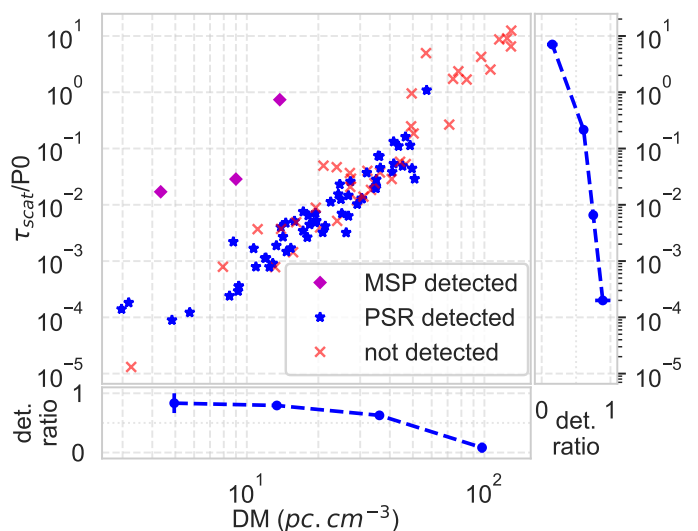
Fig. 2. Scattering time in units of the pulsar period versus the dispersion measure for the pulsars of our sample (center plot, double-logarithmic axes). Detected slow pulsars are shown as blue stars, milliseconds pulsars as magenta diamonds and non-detections as red crosses. The right and bottom panel (with semi-logarithmic axes) show the fraction of detected pulsars for each axis of the central plot.

detected in the present survey are shown as blue dots for normal pulsars and magenta diamonds for the MSPs, and non-detections are shown with red crosses. For this, pulsar distances are derived from the DM using the electron density model YMW16 (Yao et al. 2017). Only pulsars in the Galactic plane are shown (Galactic latitude between $-20°$ and $20°$).

A red isocontour denotes a dispersion measure of 100 pc cm^{-3} in the Galactic plane ($gb=0°$), corresponding to a scattering time of one second at 60 MHz (derived from the Galactic density model of Yao et al. 2017). With such a scattering delay, the pulsations even from slow pulsars are smeared out and become undetectable. Indeed, we do not have any detection beyond this isocontour. One can see that the red line is at a distance of only a few kpc of the Solar System. Indeed, low frequency observations of pulsed signal are limited to the nearby population. For comparison, it is possible to observe sources close to the Galactic center for observations at 1 GHz.

4.2. Detected pulsars

For each detected pulsar, we have measured the spin period $P0$, the DM, and the mean flux density, and we have calculated the expected scattering delay $\tau_{\rm scat}^{\rm calc}$ (derived from the Galactic density model of Yao et al. 2017). These values are detailed in Table 1.

For each detected pulsar, a single pulse profile was generated. These profiles are shown in Figure B.1. When the signal-to-noise ratio is sufficient, pulse profiles can be compared at different observing frequencies. This allows to reveal the frequency dependence of the beam pattern. This is illustrated in Figure 4 for the six pulsars with the best signal-to-noise ratio in our sample.

A mean flux density value over the entire band was obtained for each detection (Table 1). As discussed in Kon-
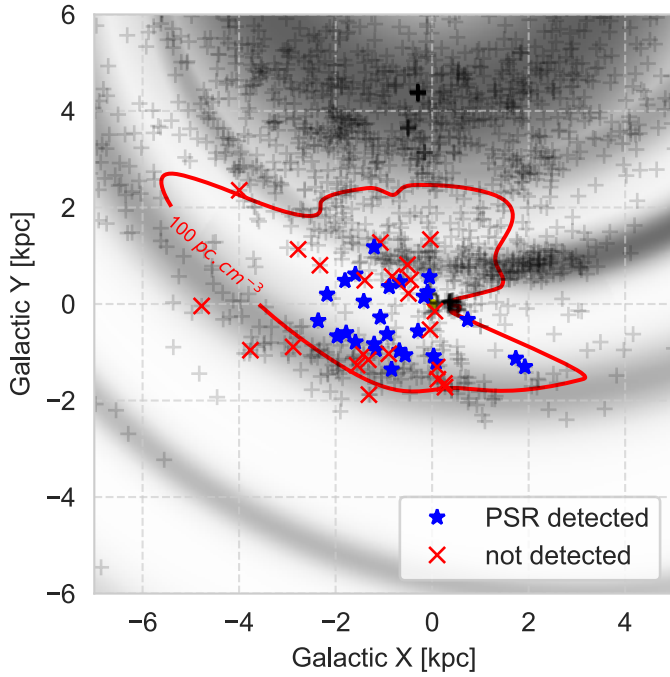
Fig. 3. Representation of the census in the Galactic plane with the Earth at the origin of the axes. The electron density model YMW16 (Yao et al. 2017) is represented in grey-scale. Blue stars: detected pulsars. Red crosses: non-detected pulsars. Only pulsars in the Galactic plane are shown (from $-20°$ to $20°$ of Galactic latitude). The red line is an isocontour for a DM of $100 \, \mathrm{pc \, cm^{-3}}$. Pulsars distances are derived from the dispersion measure using YMW16.

dratiev et al. (2016), flux calibration of beam-formed data is non-trivial due to an uncertainty of the beam shape which is dependent on the azimuth and elevation. To reflect this, the measured flux is assumed to be correct within 50%, as was recommended for LOFAR HBA observations (Bilous et al. 2016; Kondratiev et al. 2016). This error bar also includes the flux variation due to scintillation and intrinsic variability. It should be noted that this estimation was originally established for LOFAR observations in the HBA band (100-200 MHz); for observations with a single station at frequencies below 100 MHz, the situation might be slightly different. This will be studied in more detail elsewhere.
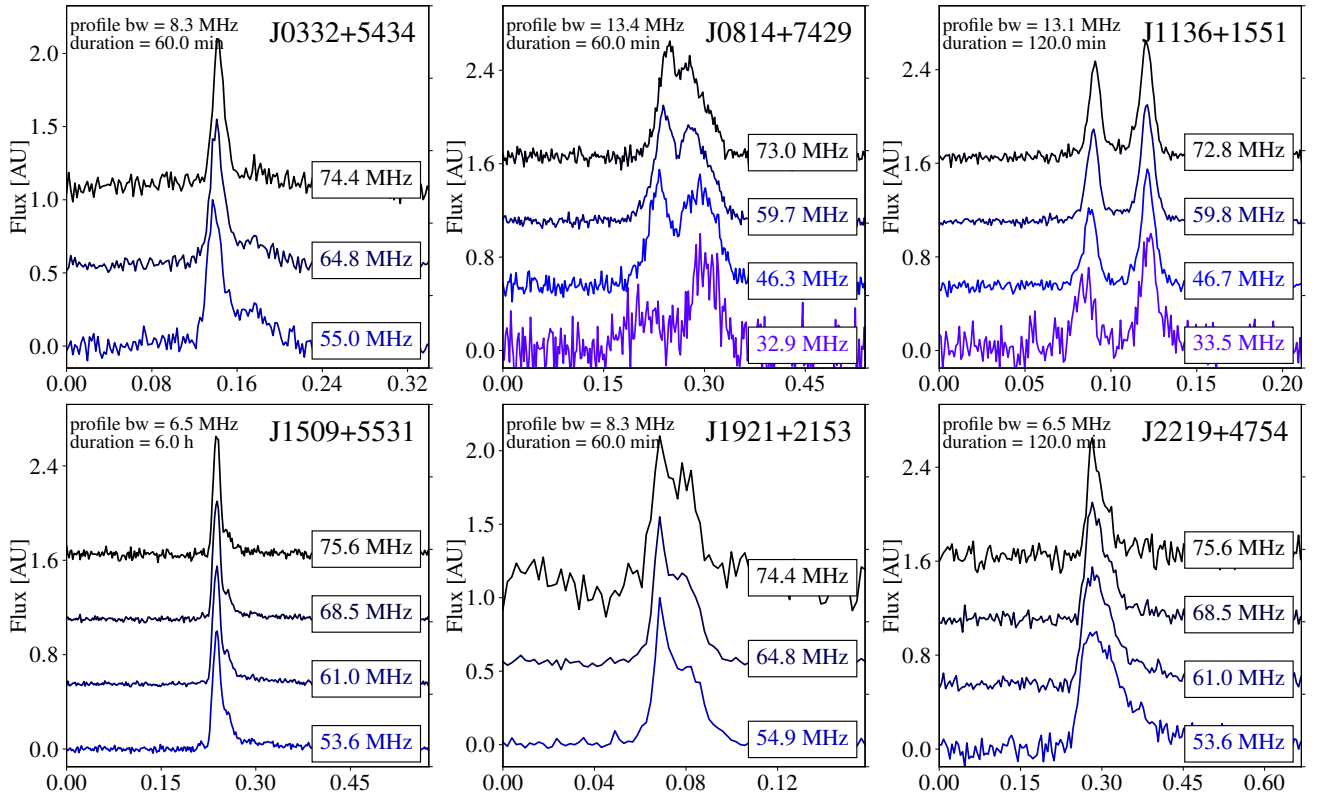
Fig. 4. Frequency-dependent profiles for the six pulsars with the best signal-to-noise-ratio in our sample. Profiles are zoomed on the on-pulse region.

JName	BName	P0 [s]	DM [pc cm^{-3}]	$\tau_{\rm scat}^{\rm calc}$/P0 [%]	duty cycle [%]	SNR	duration [min]	$f_{\rm center}$ [MHz]	avg.elev degrees	mean flux [mJy]
J0014+4746	B0011+47	1.241	30.30(2)	1.3	4.4	9	240	65	79	43(21)
J0030+0451	_	0.005	4.33320(6)	1.7	4.9	9	180	53	46	86(43)
J0034-0534	_	0.002	13.76580(4)$^\tau$	73.8	46.6	55	180	53	32	855(428)
J0034-0721	B0031-07	0.943	10.916(5)	0.1	15.3	41	120	53	35	560(280)
J0051+0423	_	0.355	13.9265(5)	0.4	5.3	14	120	53	46	30(15)
J0056+4756	B0053+47	0.472	18.14(1)	0.6	6.5	17	135	65	84	102(51)
J0108+6608	B0105+65	1.284	30.56(2)	1.3	4.0	11	325	65	67	74(37)
J0141+6009	B0138+59	1.223	34.931(2)	2.2	10.8	28	120	65	68	242(121)
J0152-1637	B0149-16	0.833	11.9289(5)	0.1	10.4	37	120	53	25	215(107)
J0323+3944	B0320+39	3.032	26.20(1)	0.3	20.8	31	165	65	73	127(63)
J0332+5434	B0329+54	0.715	26.768(1)	1.5	11.2	119	60	65	51	1841(921)
J0358+5413	B0355+54	0.156	57.15(1)$^\tau$	109	7.9	9	240	65	77	129(64)$^\sigma$
J0454+5543	B0450+55	0.341	14.5921(10)	0.5	8.7	28	325	53	53	124(62)
J0528+2200	B0525+21	3.746	50.90(2)$^\phi$	2.9	13.7	31	120	53	61	257(128)
J0611+30	_	1.412	45.31(4)	4.9	4.5	9	240	65	68	64(32)
J0630-2834	B0628-28	1.244	34.42(1)	2.0	7.9	23	55	65	14	1076(538)
J0700+6418	B0655+64	0.196	8.7749(2)	0.2	10.7	33	120	53	68	95(47)
J0814+7429	B0809+74	1.292	5.7578(9)$^\phi$	0.0	45.9	252	60	53	62	1630(815)
J0820-1350	B0818-13	1.238	40.962(10)	3.8	2.7	10	115	65	28	61(31)
J0826+2637	B0823+26	0.531	19.4743(8)	0.7	14.2	79	60	65	63	423(212)
J0837+0610	B0834+06	1.274	12.864(2)$^\phi$	0.1	6.9	309	60	65	44	1268(634)
J0908-1739	B0906-17	0.402	15.875(2)	0.5	1.5	5	180	53	24	29(15)
J0922+0638	B0919+06	0.431	27.2965(5)	2.6	15.4	144	180	65	42	550(275)
J0927+23	_	0.762	23.127(2)	0.8	0.5	6	215	62	54	12(6)
J0946+0951	B0943+10	1.098	15.3291(5)	0.2	15.2	148	150	53	46	610(305)
J0953+0755	B0950+08	0.253	2.9711(2)$^\phi$	0.0	14.6	140	60	62	41	2276(1138)
J1115+5030	B1112+50	1.656	9.197(3)	0.0	2.5	12	275	53	75	21(11)
J1136+1551	B1133+16	1.188	4.8468(7)$^\phi$	0.0	18.7	261	120	53	53	894(447)
J1238+2152	_	1.119	17.967(3)	0.3	4.1	15	155	65	62	38(19)
J1239+2453	B1237+25	1.382	9.2562(8)$^\phi$	0.0	0.2	50	170	62	65	102(51)
J1313+0931	_	0.849	12.0318(5)	0.1	2.2	7	215	57	48	25(13)
J1321+8323	B1322+83	0.670	13.28(3)	0.2	1.4	5	225	53	43	16(8)
J1509+5531	B1508+55	0.740	19.616(1)	0.5	10.7	378	360	65	73	943(471)
J1532+2745	B1530+27	1.125	14.697(6)	0.1	6.0	18	240	53	66	69(35)
J1543-0620	B1540-06	0.709	18.372(4)	0.4	9.0	22	145	65	34	143(72)
J1543+0929	B1541+09	0.748	34.950(5)	3.5	5.6	26	90	53	50	541(270)
J1607-0032	B1604-00	0.422	10.6823(5)	0.2	9.9	64	60	53	42	575(288)
J1614+0737	B1612+07	1.207	21.401(2)	0.4	3.8	24	165	65	48	120(60)
J1635+2418	B1633+24	0.491	24.24(1)	1.5	3.9	8	210	65	56	68(34)
J1645-0317	B1642-03	0.388	35.7589(5)	7.4	8.8	48	240	65	37	420(210)
J1645+1012	_	0.411	36.165(6)	7.3	4.6	12	165	65	50	108(54)
J1709-1640	B1706-16	0.653	24.892(2)	1.3	7.3	17	120	53	25	317(159)
J1740+1311	B1737+13	0.803	48.660(5)$^\tau$	11.3	4.6	14	180	65	36	131(66)

Continued on next page

Continued from previous page

JName	BName	P0 [s]	DM [pc cm^{-3}]	$\tau_{\text{scat}}^{\text{calc}}$/P0 [%]	duty cycle [%]	SNR	duration [min]	f_{center} [MHz]	avg.elev degrees	mean flux [mJy]
J1741+2758	_	1.361	29.168(8)	1.0	9.6	21	210	65	67	54(27)
J1758+3030	_	0.947	35.08(1)	2.8	2.0	8	115	65	67	26(13)
J1813+4013	B1811+40	0.931	41.60(2)	5.4	2.1	11	115	65	57	68(34)
J1825-0935	B1822-09	0.769	19.386(2)	0.5	5.7	33	120	53	32	2502(1251)
J1840+5640	B1839+56	1.653	26.773(2)	0.6	7.0	166	180	65	57	481(240)
J1844+1454	B1842+14	0.375	41.483(2)$^\tau$	13.2	6.7	36	120	65	51	773(386)
J1921+2153	B1919+21	1.337	12.437(2)	0.1	8.4	180	60	65	63	1586(793)
J1932+1059	B1929+10	0.227	3.186(2)	0.0	5.8	15	120	53	41	306(153)
J1955+5059	B1953+50	0.519	31.990(5)	3.7	1.2	5	225	65	70	16(8)
J2018+2839	B2016+28	0.558	14.1982(5)	0.3	8.6	37	135	53	54	243(121)
J2022+2854	B2020+28	0.343	24.6315(10)	2.3	6.2	30	150	65	69	243(122)
J2022+5154	B2021+51	0.529	22.541(6)	1.1	1.3	6	120	65	81	46(23)
J2113+2754	B2110+27	1.203	25.121(3)	0.7	8.4	37	150	65	65	143(71)
J2145-0750	_	0.016	9.0058(2)	2.9	3.5	8	180	53	34	59(30)
J2219+4754	B2217+47	0.538	43.492(1)$^\tau$	11.0	15.6	125	120	65	76	1239(620)
J2225+6535	B2224+65	0.683	36.473(4)	4.5	5.5	29	210	65	46	293(146)
J2305+3100	B2303+30	1.576	49.60(3)	6.2	4.1	11	115	65	72	45(22)
J2308+5547	B2306+55	0.475	46.57(4)$^\tau$	16.2	2.3	5	120	65	70	170(85)
J2313+4253	B2310+42	0.349	17.282(8)	0.8	2.6	11	240	65	60	81(41)
J2317+2149	B2315+21	1.445	20.876(5)	0.3	3.7	10	120	65	59	35(18)
J2330-2005	B2327-20	1.644	8.4554(10)	0.0	4.0	16	120	53	22	111(55)

Table 1. Pulsars detected in this census. JName, BName: pulsar name. P0: pulsar period. DM: the best-fit DM calculated using `pdmp`. $\tau_{\text{scat}}^{\text{calc}}$/P0: the scattering time (as estimated using YMW16, Yao et al. 2017, at 60 MHz) divided by the pulsar period, expressed in %. duty cycle: the effective width in pulses profiles (based on w50), expressed in %. SNR: the signal-to-noise-ratio of the detected pulsar profile. duration: total observation length in minutes. f_{center}: the center frequency of the observation in MHz. avg.elev: the average elevation during the observation. mean flux: the mean flux density determined for the corresponding center frequency, with an error bar of 50%. $^\sigma$: pulsed flux density only (due to scatter broadening, part of the pulsar's energy reaches the telescope as continuum, see Section 5.2). $^\tau$: the dispersion measure is not corrected for the effect of scatter-broadening (see Section 5.1). $^\phi$: the dispersion measure is not corrected for the effect of intrinsic profile evolution with frequency (see Section 5.1).

4.3. Upper limits for non-detections

For each non-detection, we have computed an upper limit for the mean flux density according to Equation (1) in Section 3.6. The resulting values are given in Table A.1. Depending on source position and observation time, we obtain upper limits between ~ 60 and 4500 mJy, which is compatible with our initial expectation (Figure 1).

Compared to previous observations, only 20 pulsars previously detected below 100 MHz have either not been observed or not been detected. Of these, one (J0437-4715) is not observable for FR606, and 7 others have not been observed as part of this survey. This leaves 13 previously reported pulsars which we have not detected, some of which were reported as faint or marginal detections:

- J0231+7026 was detected by the LOFAR core LBA census (Bilous et al. 2019) with a mean flux density of 49 mJy, which is consistent with our upper limit of 329 mJy.
- J0304+1932 has been reported by Izvekova et al. (1981, $\sim$40 mJy at 61 MHz), by Stovall et al. (2015, 120±60 mJy at 64.5 MHz), and has been detected in the LOFAR core LBA census (Bilous et al. 2019, 61±33 mJy at 50 MHz). Our upper limit is 121 mJy, which is compatible with all of these detections.
- J0612+3721 was detected by the LOFAR core LBA census (Bilous et al. 2019) with a mean flux density of 46 mJy, which is consistent with our upper limit of 664 mJy.
- J0614+2229 was previously reported as a detection (Izvekova et al. 1981, 180 mJy at 85 MHz), which is compatible with our upper limit of 337 mJy.
- J0659+1414 was a reported with a very low flux density ($\sim$60 mJy at 85 MHz, Izvekova et al. 1981), which is compatible with our upper limit of 77 mJy.
- We expected to detect J0921+6254 (detected in Pilia et al. 2016, but no measured flux density). The pulsar was detected by the LOFAR core LBA census (Bilous et al. 2019) with a mean flux density of 41±22 mJy, which is consistent with our upper limit of 58 mJy.
- J0943+1631 was a weak detection in Zakharenko et al. (2013), which is compatible with our upper flux limit.
- J1752-2806 has been reported twice (Izvekova et al. 1981; Stovall et al. 2015), but is at very low elevation for FR606, which strongly reduced the efficiency of the antenna array. This is reflected in our little constraining upper limit of 4533 mJy, which is compatible with the previous detections.
- J1841+0912 was detected by the LOFAR core LBA census (Bilous et al. 2019) with a mean flux density of 190 mJy, which is consistent with our upper limit of 521 mJy.
- J1851-0053 was a weak detection in Zakharenko et al. (2013, 7 mJy at 25 MHz), compatible with our upper flux limit of 578 mJy.
- J1908+0734 was a weak detection in Zakharenko et al. (2013, 7 mJy at 25 MHz), compatible with our upper flux limit of 203 mJy.
- Based on Zakharenko et al. (2013, 27 mJy at 25 MHz), we hoped to detect J1946+1805 for which we have an upper limit of 110 mJy, but the non-detection is compatible within the error bars.

- Based on Zakharenko et al. (2013, 15 mJy at 25 MHz), we hoped to detect J1954+2923 for which we have an upper limit of 124 mJy, but the non-detection is compatible within the error bars.

Besides lack of sensitivity, other possible reasons for non-detections are discussed in Section 5.6.

5. Discussion

5.1. Dispersion at low frequency

In Section 4.2, we have presented DM values for all pulsars detected in this census. To obtain these values, we have used `pdmp` which modifies the DM value until the signal-to-noise ratio of the pulse profile is maximized.

This approach does not correctly take into account frequency-dependent pulse profile variations. A typical example for this would be a pulsar with two or more bright components, whose flux ratio changes as a function of frequency such as B1133+16 and B0809+74 (cf. Figure 4).

A similar situation arises for pulsars that are scatter-broadened. In that case, part of the scatter-broadening ($\propto f^{-4}$) is absorbed by `pdmp`, resulting in an erroneous extra correction of the DM ($\propto f^{-2}$), especially at low frequencies.

An ideal dedispersion process should use a 2D template, either based on Gaussian fits (Pennucci et al. 2014) or based on the smoothed dataset (e.g. Donner et al. 2019). In addition, a fiducial point would be required (e.g. Hassall et al. 2012) in order to disentangle dispersion and frequency-dependent profile variation. Without this, the absolute DM cannot be measured.

We did not apply any of these methods in this publication, which limits the DM precision for some of the pulsars in this census. These pulsars are clearly labelled in Table 1.

5.2. Dispersion, scattering and detection rate

As discussed in Section 4.1, dispersion and scattering are correlated. Indeed, Figure 2 shows that the measured DM and the calculated scattering time from YMW16 (calculated using Yao et al. 2017) are correlated in our sample of detected pulsars. The detection rates decrease for high scattering time and high DM. Low frequency observations are highly affected by the dispersion introduced by the interstellar medium. However, this effect is corrected using coherent dedispersion (Hankins & Rickett 1975; Bondonneau et al. 2019).

Consequently, the low detection rate in high DM is not due to the dispersion, but caused by the multi-path propagation in the interstellar medium which is usually described by a convolution between the pulse profile and an exponential function. The result is an exponential tail characterized by the scattering time τ, as can be seen e.g. for J2219+4754 in Figure B.1. For some pulsars the scattering time is larger than the rotational period and the pulsations disappear during the folding process. This is the reason why some of the targets (J0324+5239, B0531+21, B0540+23, B0611+22, B0626+24, B1931+24, B1946+35, B2148+63 and B2227+61) are not detected: their scattering time exceeds the pulsar's period, cf. Figure 2 and Table A.1.

For B0355+54, the estimated scattering time slightly exceeds the pulse period (Table 1). With this, the pulsar

should still remain visible, which is indeed the case (see Figure B.1). As part of the pulsar's energy reaches the telescope as continuum rather than pulsed emission, the measured flux density only represented the pulsed flux.

We have compared the scattering times obtained with YMW16 (Yao et al. 2017) to those given by a different Galactic density model, NE2001 (Cordes & Lazio 2002). The latter model seems to underestimate the scattering with respect to YMW16 and to the value deduced from our own observed profiles (Figure B.1). This is true in particular for J0358+5413, B2217+47 and B2306+55, where the values given by NE2001 are respectively 11.6%, 1.4% and 3.4% of the phase, numbers that are far away from those extracted from our own observed profiles or from the values provided by the electron density model YMW16, namely 108.7%, 11.0% and 16.2% (cf. Table 1, column 5).

Note that for some pulsars, the measured scattering index α_{scat} (defining the frequency dependence of the scattering time τ_{scat}) obtained from observations can deviate considerably from the theoretical value of 4.0 or 4.4 used in models such as Yao et al. (2017). In particular, Geyer et al. (2017) analysed LOFAR observations at 150 MHz and found a less steep behavior for J0117+5914, J0543+2329 and J0614+2229. If this is confirmed and can be extended to our observing frequency of 60 MHz, the resulting scattering time would be lower, and the pulsars would not be rendered undetectable by scattering. In that case, the non-detection of these specific targets would be caused by a different reason (see e.g. Section 5.6).

5.3. Spectral turnover: comparison with HBA census (110-188 MHz)

39 pulsars of the FR606 LBA census (25-80 MHz) described in this publication have also been detected in the LOFAR HBA census (Bilous et al. 2016, 110-188 MHz). The spectral index and turnover frequency given in Bilous et al. (2016) can be used to estimate a theoretically expected mean flux density for the LBA frequency range and to compare it to our measurements.

Figure 5 compares the mean flux densities obtained from the present LBA census (X-axis) to the theoretical mean flux density extrapolated from Bilous et al. (2016) (Y-axis). Pulsars are represented with a blue dot if Bilous et al. (2016) identified a turnover, and a red triangle otherwise (i.e. the spectrum was fitted using only one spectral index). For FR606 observations, we indicate the nominal error resulting from the flux calibration. The systematic error of 50% is represented by the blue/green surface around the diagonal line of equal fluxes.

For most pulsars, the measured and the extrapolated mean flux densities agree within the error range. The exceptions are the following:

- For a five pulsars (J0611+30, J0700+6418, J1313+0931, J1645+1012 and J1955+5059), the mean flux density extrapolated from the HBA range is considerably higher than the flux density we measured in the LBA range. For these pulsars, Bilous et al. (2016) give a simple power-law without turnover. Our observations show a considerable lack of flux density below 100 MHz, indirectly showing that these pulsars do indeed have a spectral turnover at low frequencies.

- Similarly, but with a lower significance, we see a hint for a turnover for J2219+4754 (B2217+47).
- For J1115+5030 (B1112+50), the extrapolated flux is overestimated with respect to the measurement. It is, however, consistent with the HBA flux measured in in Bilous et al. (2016). The extrapolation takes this HBA flux into account, but also (older) literature values, suggesting possible time variability of this pulsar.
- For J1239+2453 (B1237+25), the expected mean flux density is overestimated even though Bilous et al. (2016) fit a spectral turnover. The model uses three frequency ranges with different spectral indices. We suspect that the turnover happens at slightly higher frequency than the 45 MHz estimated in Bilous et al. (2016).
- For J2022+2854 (B2020+28) the spectral index of the extrapolation is not well constrained. A shallower spectral index at low frequencies is compatible with both previous observations and our LBA data.

This comparison of observations at frequencies below 100 MHz (our work) to observations above 100 MHz (Bilous et al. 2016) shows that several pulsars which used be described using a single power-law have a spectral turnover. This does not come unexpected: Bilous et al. (2016) found that the average spectral index is lower for measurements at 150 MHz than for higher frequencies (potentially indicating proximity to a turnover), and noted that measurements below 100 MHz are required to study the phenomenon of turnover systematically.

For a number of pulsars which were modelled without spectral turnover (Bilous et al. 2016), our measured flux density is in agreement with the extrapolated flux density value. This indicates that these pulsars either have no turnover, or (more likely) the turnover occurs at frequencies below our sensitivity maximum (~ 58 MHz). Again, more high sensitivity observations below 100 MHz are required for a systematic study.

The comparison presented above is just a first step. A detailed analysis of spectral indices and turnover frequencies will be presented in a companion publication for the brightest pulsars in our sample (Bondonneau et al., 2019, in prep.), and more sensitive observations will be provided by NenuFAR in the near future.

5.4. Comparison with the LOFAR LBA census

In a companion study, we observed pulsars with the LBA antennas of the LOFAR core (Bilous et al. 2019). Between both studies, there are in total 64 common targets. Of these, 36 targets were detected by both FR606 and the LOFAR core, 5 were detected only by the LOFAR core, 1 was detected only by FR606, and 22 were not detected by either instrument.

Common detections   Figure 6 shows the measured flux densities from the LOFAR Core LBA census (Y-axis) reported by Bilous et al. (2019) in comparison with the flux density measurements from the current FR606 census (X-axis). For FR606 and LOFAR Core observations, we indicate the nominal error resulting from the flux calibration. The systematic error of 50% is represented by the blue/green surface around the diagonal line of equal fluxes.

For all of the 36 pulsars that were detected in both censuses, the measured flux densities are compatible or al-

most compatible within the uncertainties. Some of the values are not matching perfectly (e.g. B1508+55, B1919+21, B1929+10). This can have a number of reasons (see, e.g., Kondratiev et al. 2016), such as the contribution of strong background sources to the wide low-frequency beam, beam jitter caused by the ionosphere, refractive scintillation (RISS), or intrinsic variability. Each of these factors can increase or decrease the measured flux density. For instance, both censuses were performed at different epochs, so that RISS could affect the measurements differently. For the pulsars B1508+55 and B2020+28, FR606 has measured a slightly higher flux density than the LOFAR core. This could be explained by ionosphere jitter during the LOFAR Core census observations (the field-of-view of the international station is wider, so that a small shift of the beam should not matter for our FR606 observations). Indeed, Bilous et al. (2019) used multiple beams simultaneously and found a higher flux density in one of the off-center beams for several pulsars (including B1508+55).

The same factors could potentially lead to non-detections by one of the telescopes, or both. Figure 6 includes pulsars detected by at least one of the telescopes. In case of non-detection by one of the telescopes, we use the upper limit value on flux density.

Pulsars detected only by LOFAR core Five of the pulsars seen with the LOFAR Core have not been detected by FR606, namely PSRs B0226+70, B0301+19, B0609+37, B0917+63, and B1839+09. For all of these non-detections, the upper limits deduced from our FR606 observations are compatible with the measured flux densites of the LOFAR core (see Figure 6). The non-detection of B0917+63 by FR606 in 275 minutes came as a bit of surprise. It is possible that RISS lead to intensity variations. Still, the upper limit of FR606 is compatible with the measured flux density from the LOFAR core.

Pulsars detected only by FR606 PSR J1741+2758 was not detected with the LOFAR Core in 23 minutes, while it was detected by FR606 in 210 minutes. The smaller effective area of FR606 (96 dipoles of FR606 vs. 24x48 dipoles of the Core) is balanced out by the longer integration time. Also, for the LOFAR Core observation, this particular dataset was of poor quality (more than half of the band was deleted due to dropped packets, see Bilous et al. 2019).

The non-detection by the LOFAR Core yields an upper flux density limit which is compatible with the detection by FR606. Also, note that this pulsar had already been detected at frequencies below 100 MHz before (Zakharenko et al. 2013).

5.5. Millisecond pulsars

Currently, radio detections at frequencies below 100 MHz have been published for four millisecond pulsars (Dowell et al. 2013; Kondratiev et al. 2016; Bhat et al. 2018), of which three are observable by FR606. We have observed and detected all three of these targets. In view of the low flux densities of these targets, we did not include any other millisecond pulsars in our sample.

5.6. Possible reasons for non-detections

There are a number of potential reasons for non-detections:

- The spectrum (as characterized by the spectral index + turnover) is not favourable for very low frequency observations.
- The pulse period is outside the range of values probed by `pdmp`. All of our targets have been previously detected below 200 MHz, so we expect the range of DM values to be large enough. For the search range in pulsar period, we have probed all values which result in pulse smearing <1.5% of one period per subintegration with respect to the nominal period. In the unlikely case of a period outside this search window, the pulsar may remain undetected.
- The pulse is smeared by scatter-broadening. This is the case, for example, for the Crab pulsar B0531+21, for which the scattering time is about 500% of the pulse period. For a number of the pulsars in Table A.1, the expected scatter broadening is high ($\tau_{\mathrm{scat}}^{\mathrm{calc}}/P0 > 1$), which is indeed compatible with our non-detection. See Section 5.2 for details.
- Intermittent emission such as nulling or mode changing can affect a pulsars detectability. For example, B0943+10 (Hermsen et al. 2013; Bilous et al. 2014) and B0823+26 (Sobey et al. 2015) are known for their mode changing behavior at low frequencies. For mode-changing pulsars, the mean flux density depends on the state of the pulsar during the observation, which can make the different between a detection and a non-detection. The same is, of course, true for nulling pulsars.
- Diffractive scintillation should not affect our measurements because the decorrelation bandwidths should be lower than our bandwidth, so that many scintles are averaged out.
- Slow fluctuations of the pulsar amplitudes can be caused by refractive scintillation by the interstellar medium. For observations at 74 MHz, Gupta et al. (1993) measured modulation indices (ratio of the standard deviation of the observed flux densities to their mean) in the range 0.15-0.45, which can account for some of our non-detections. The bandwidth they used was of 500 kHz, which is much less than our bandwidth. However, refractive scintillation is broadband in nature (Narayan 1992), so that bandwidth should not matter.
- Some of the flux density values given in earlier publications can be over-estimations, especially in cases with a low signal-to-noise ratio.

6. Conclusion

In this publication, we observed a total of 102 pulsars, out of which 64 were detected successfully. Two of these have never been detected at frequencies below 100 MHz before.

We obtained results similar to the companion study using the LOFAR core (Bilous et al. 2019). We were able to partially compensate the lower effective area (∼10%) by longer integrations during RFI-quiet moments (thus optimising the quality data). Due to the lower sensitivity of FR606, we did not detect all pulsars detected by Bilous et al. (2019), but our upper limits are compatible with their flux density measurements. We detected two pulsars that were not part of the sample of Bilous et al. (2019), and

one pulsar (J1741+2758) that was a non-detection in that study.

For several pulsars (J0611+30, J0700+6418, J1313+0931, J1645+1012 and J1955+5059), the comparison to observations at slightly higher frequencies (Bilous et al. 2016) indicates a previously unknown spectral turnover. This confirms the expectation that spectral turnovers are a wide-spread phenomenon, and that measurements below 100 MHz are essential to study this phenomenon systematically.

It should be noted that the pulsar population represented in this census is biased by the selection method, essentially based on previous detections of (Stovall et al. 2015; Pilia et al. 2016; Kondratiev et al. 2016; Bilous et al. 2016). It does not allow new low frequency detection if the pulsar has not been detected in the HBA range.

In order to further study the population statistics of these low-frequency pulsars, a more homogeneous and substantial dataset is required. This will be reached by the NenuFAR radio telescope (Zarka et al. 2012, 2014, 2015) and its pulsar instrumentation LUPPI (Bondonneau et al. 2019), with which we are currently conducting a systematic census of the pulsar population (Bondonneau et al. in prep). NenuFAR, while providing us with an equivalent sensitivity to the LOFAR core at 60 MHz, offers a flat gain response across the LBA frequency band (from 10-85 MHz). Consequently, a much higher detection rate can be expected than for the present census. In addition, the flat frequency response will allow a much higher sensitivity towards frequency-dependent effects such as dispersion, scattering, spectral turnovers, and pulsar profile evolution.

References

Bhat, N. D. R., Cordes, J. M., Camilo, F., Nice, D. J., & Lorimer, D. R. 2004, The Astrophysical Journal, 605, 759

Bhat, N. D. R., Tremblay, S. E., Kirsten, F., et al. 2018, The Astrophysical Journal Supplement Series, 238, 1, arXiv: 1807.06989

Bilous, A., Kondratiev, V., Kramer, M., et al. 2016, Astronomy & Astrophysics, 591, A134, arXiv: 1511.01767

Bilous, A. V., Bondonneau, L., Kondratiev, V. I., Grießmeier, J.-M., et al. 2019, A&A, to be submitted

Bilous, A. V., Hessels, J. W. T., Kondratiev, V. I., et al. 2014, Astronomy & Astrophysics, 572, A52

Bondonneau, L., Grießmeier, J., Theureau, G., Cognard, I., & the NenuFAR-France collaboration. 2019, in Journées scientifiques 2019 d'URSI-France, 1–8

Bondonneau, L., Grießmeier, J.-M., Theureau, G., & Serylak, M. 2018, Pulsar Astrophysics the Next Fifty Years, 337, 313

Cordes, J. M. 1978, Astrophys. J., 222, 1006

Cordes, J. M. & Lazio, T. J. W. 2002, arXiv:astro-ph/0207156, arXiv: astro-ph/0207156

Deshpande, A. A. & Radhakrishnan, V. 1992, J. Astrophys. Astr., 13, 151

Dicke, R. H. 1946, Review of Scientific Instruments, 17, 268

Donner, J. Y., Verbiest, J. P. W., Tiburzi, C., et al. 2019, A&A, 624, A22

Dowell, J., Ray, P. S., Taylor, G. B., et al. 2013, The Astrophysical Journal, 775, L28

Geyer, M., Karastergiou, A., Kondratiev, V. I., et al. 2017, Mon. Not. R. Astron. Soc., 470, 4659

Grießmeier, J.-M., Bondonneau, L., Serylak, M., & Theureau, G. 2018, Pulsar Astrophysics the Next Fifty Years, 337, 338

Gupta, Y., Rickett, B. J., & Coles, W. A. 1993, Astrophys. J., 403, 183

Hamaker, J. P. 2006, A&A, 456, 395

Hankins, T. H. & Rickett, B. J. 1975, Methods in Computational Physics. Volume 14 - Radio astronomy, 14, 55

Haslam, C. G. T., Salter, C. J., Stoffel, H., & Wilson, W. E. 1982, Astron. Astrophys. Suppl. Ser., 47, 1

Hassall, T. E., Stappers, B. W., Hessels, J. W. T., et al. 2012, Astronomy & Astrophysics, 543, A66

Hermsen, W., Hessels, J. W. T., Kuiper, L., et al. 2013, Science, 339, 436

Hermsen, W., Kuiper, L., Basu, R., et al. 2018, Mon. Not. R. Astron. Soc., 480, 3655

Hotan, A. W., van Straten, W., & Manchester, R. N. 2004, Publications of the Astronomical Society of Australia, 21, 302

Izvekova, V. A., Kuzmin, A. D., Malofeev, V. M., & Shitov, Y. P. 1981, Astrophys. Space Sci., 78, 45

Kondratiev, V. I., Verbiest, J. P. W., Hessels, J. W. T., et al. 2016, Astronomy & Astrophysics, 585, A128

Lawson, K. D., Meyer, C. J., Osborne, J. L., & Parkinson, M. L. 1987, Mon. Not. R. Astron. Soc., 225, 307

Lazarus, P., Karuppusamy, R., Graikou, E., et al. 2016, Monthly Notices of the Royal Astronomical Society, 458, 868

Lorimer, D. & Kramer, M. 2004, Handbook Of Pulsar Astronomy

Manchester, R. N., Hobbs, G. B., Teoh, A., & Hobbs, M. 2005, Astron. J., 129, 1993

Mereghetti, S., Kuiper, L., Tiengo, A., et al. 2016, Astrophys. J., 831, 21

Mereghetti, S., Kuiper, L., Tiengo, A., et al. 2018, in IAU Symp. 337: Pulsar Astrophysics - The Next 50 Years, ed. P. Weltevrede, B. Perera, L. L. Preston, & S. Sanidas, 62–65

Michilli, D., Hessels, J. W. T., Donner, J. Y., et al. 2018a, Monthly Notices of the Royal Astronomical Society, 476, 2704, arXiv: 1802.03473

Michilli, D., Hessels, J. W. T., Donner, J. Y., et al. 2018b, Pulsar Astrophysics the Next Fifty Years, 337, 291

Narayan, R. 1992, Phil. Trans. R. Soc. Lond. A, 341, 151

Pennucci, T. T., 2, P. B. D., & Ransom, S. M. 2014, Astrophys. J., 790, 93

Pilia, M., Hessels, J. W. T., Stappers, B. W., et al. 2016, Astronomy & Astrophysics, 586, A92

Rajwade, K., Seymour, A., Lorimer, D. R., et al. 2016, Mon. Not. R. Astron. Soc., 462, 2518

Reyes, F., Carr, T. D., Oliver, J. P., et al. 1980, R. Mexicana Astron. Astrof., 6, 219

Ruderman, M. & Sutherland, P. 1975, Theory of pulsars: polar gaps, sparks, and coherent microwave radiation

Smith, D. A., Bruel, P., Cognard, I., et al. 2019, The Astrophysical Journal, 871, 78

Sobey, C., Young, N. J., Hessels, J. W. T., et al. 2015, Mon. Not. R. Astron. Soc., 451, 2493

Stappers, B. W., Hessels, J. W. T., Alexov, A., et al. 2011, Astronomy & Astrophysics, 530, A80

Stovall, K., Ray, P. S., Blythe, J., et al. 2015, The Astrophysical Journal, 808, 156

Tiburzi, C., Verbiest, J. P. W., Shaifullah, G. M., et al. 2019, Monthly Notices of the Royal Astronomical Society, 487, 394, arXiv: 1905.02989

van Haarlem, M. P., Wise, M. W., Gunst, A. W., et al. 2013, Astronomy & Astrophysics, 556, A2

van Straten, W. & Bailes, M. 2011, Publications of the Astronomical Society of Australia, 28, 1

Wijnholds, S. J. & van Cappellen, W. A. 2011, IEEE Trans. Antennas Propagat., 59, 1981

Yao, J. M., Manchester, R. N., & Wang, N. 2017, The Astrophysical Journal, 835, 29

Zakharenko, V. V., Vasylieva, I. Y., Konovalenko, A. A., et al. 2013, Monthly Notices of the Royal Astronomical Society, 431, 3624

Zarka, P., Girard, J. N., Tagger, M., Denis, L., & the LSS team. 2012, in SF2A-2012: Semaine de l'Astrophysique Francaise, 687–694

Zarka, P., Tagger, M., Denis, L., et al. 2015, in International Conference on Antenna Theory and Technique, 13–18

Zarka, P., Tagger, M., et al. 2014, NenuFAR: instrument description and science case, Tech. rep., https://www.researchgate.net/publication/308806477_NenuFAR_Instrume
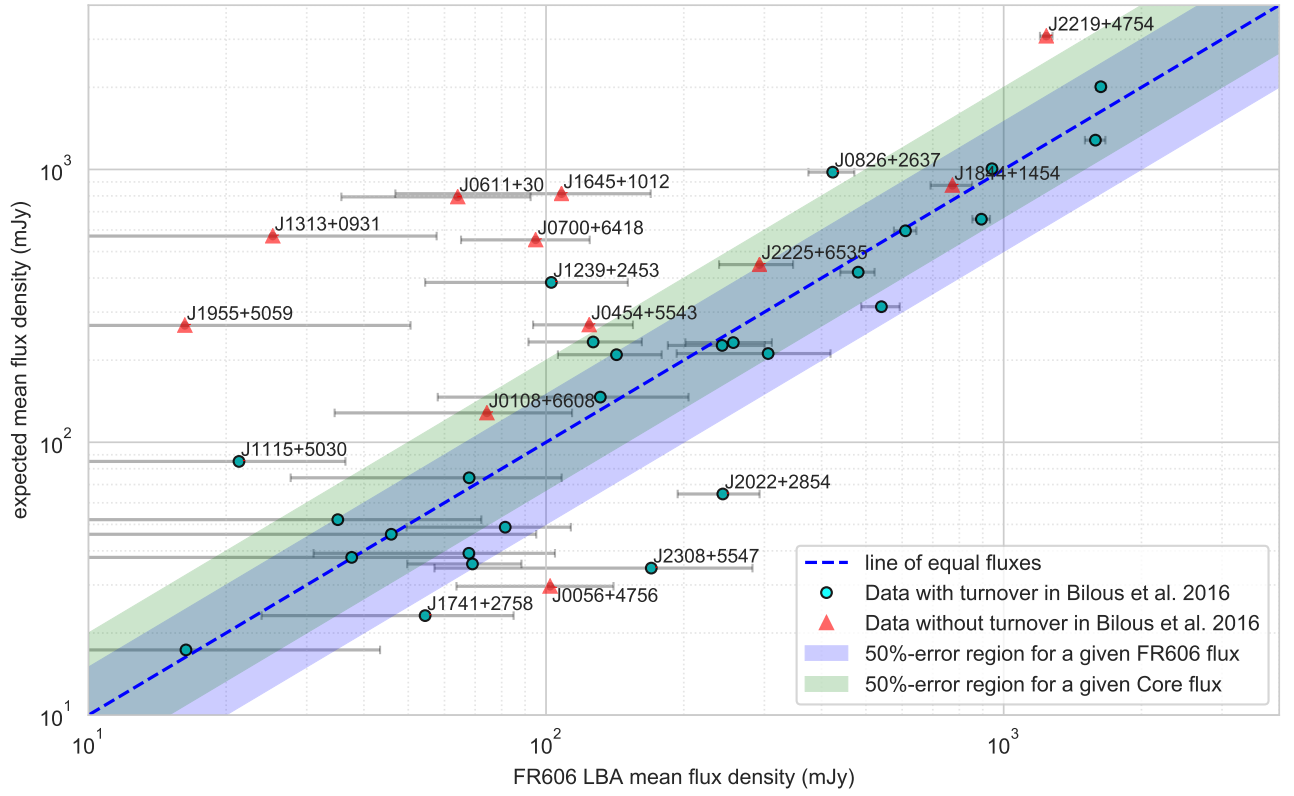
Fig. 5. Comparison of the mean flux densities reported in this paper with those obtained from the fitted spectral indices in Bilous et al. (2016). The line of equal flux values is shown by blue dashed line. Blue area shows the 50%-error region for the extrapolated Core flux densities when FR606 flux density is fixed. The green area shows the 50%-error region for the FR606 flux densities for a fixed extrapolated Core flux. Thus, effectively both regions taken together cover the area from 50% to 200% of the line of equal flux densities. Blue dots: pulsars fitted with at least one turnover in their spectrum. Red triangles: pulsars fitted with a single spectral index.
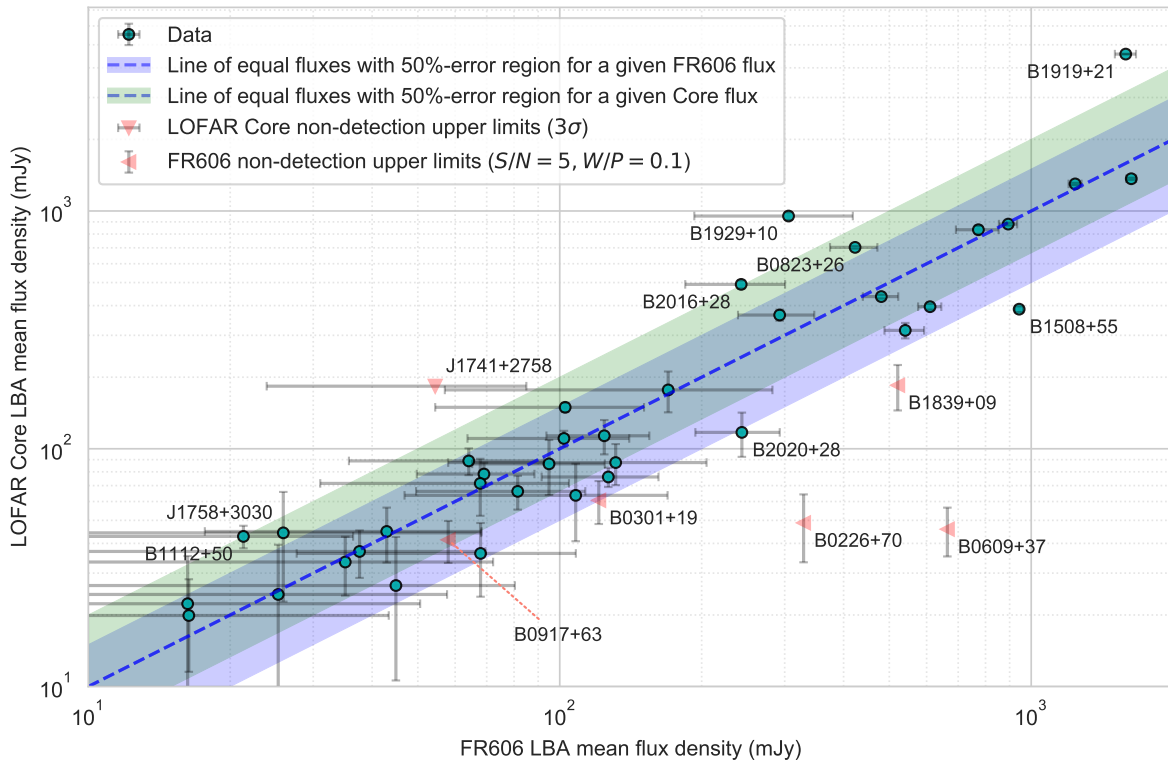
Fig. 6. Comparison of the mean flux densities reported in this paper with those obtained by Bilous et al. (2019). The line of equal flux values is shown by blue dashed line. Blue area shows the 50%-error region for the Core flux densities when FR606 flux density is fixed. The green area shows the 50%-error region for the FR606 flux densities for a fixed Core flux. Thus, effectively both regions taken together cover the area from 50% to 200% of the line of equal flux densities. Red triangles show the flux density upper limits when a pulsar was detected only by FR606 LBA (triangle is pointing down), or only by LOFAR Core (triangles are pointing left). Note that for the upper limits for the LOFAR Core we used the value of 3σ, where σ is the nominal uncertainty on the flux following Bilous et al. (2016) (Vlad, can you explain?) , while for FR606 upper limits we used Equation (1) from the present paper.

Appendix A: Non-detection Table

JName	BName	P0 sec	DM pc.cm^{-3}	$\tau_{\text{scat}}^{\text{calc}}$/P0 %	duration min	elev degree	upper limit for the mean flux density [mJy]
J0117+5914	B0114+58	0.1014	49.4230	95.3	255	64	344$^\tau$
J0139+5814	B0136+57	0.2725	73.7790	172.6	225	63	366$^\tau$
J0231+7026	B0226+70	1.4668	46.6400	5.3	240	45	329
J0304+1932	B0301+19	1.3876	15.7370	0.1	240	53	121
J0324+5239	_	0.3366	119.0000	984.6	240	56	281$^\tau$
J0415+6954	B0410+69	0.3907	27.4650	2.9	360	44	253
J0534+2200	B0531+21	0.0334	56.7875	497.4	60	43	705$^{\eta,\tau}$
J0543+2329	B0540+23	0.2460	77.7115	235.8	120	61$^\tau$	428$^\tau$
J0612+3721	B0609+37	0.2980	27.1350	3.7	110	42	664
J0614+2229	B0611+22	0.3350	96.9100	426.0	240	61	337$^\tau$
J0629+2415	B0626+24	0.4766	84.1950	168.4	180	48	540$^\tau$
J0653+8051	B0643+80	1.2144	33.3320	1.8	240	56	316
J0659+1414	B0656+14	0.3849	13.9770	0.4	240	53	77
J0921+6254	B0917+63	1.5680	13.1580	0.1	275	51	58
J0943+1631	B0940+16	1.0874	20.3200	0.4	115	58	430
J0943+22	_	0.5329	25.1000	1.6	360	65	24
J0947+27	_	0.8510	29.0000	1.6	220	65	1344
J1503+2111	_	3.3140	3.2600	0.0	360	48	57
J1612+2008	_	0.4266	19.5440	0.9	240	56	298
J1627+1419	_	0.4909	33.8000	4.8	180	55	415
J1649+2533	_	1.0153	35.5000	2.8	240	64	303
J1720+2150	_	1.6157	41.1000	3.0	240	57	292
J1740+1000	_	0.1541	23.8500	4.6	120	43	501
J1752-2806	B1749-28	0.5626	50.3720	18.5	60	14	4533
J1841+0912	B1839+09	0.3813	49.1070	24.8	120	50	521
J1851-0053	_	1.4091	24.0000	0.5	240	38	578
J1907+4002	B1905+39	1.2358	30.9600	1.4	250	53	262
J1908+0734	_	0.2124	11.1040	0.4	360	45	203
J1933+2421	B1931+24	0.8137	105.9251	252.3	120	64	468$^\tau$
J1946+1805	B1944+17	0.4406	16.2200	0.5	120	59	110
J1948+3540	B1946+35	0.7173	129.0750	646.7	120	77	391$^\tau$
J1954+2923	B1952+29	0.4267	7.9320	0.1	115	54	124
J2043+2740	_	0.0961	21.0000	4.9	115	56	425
J2055+2209	B2053+21	0.8152	36.3610	3.8	120	64	419
J2139+2242	_	1.0835	44.1000	5.8	115	57	427
J2149+6329	B2148+63	0.3801	128.0000	1178.8	120	72	1798$^\tau$
J2157+4017	B2154+40	1.5253	70.8570	26.2	180	36	399
J2229+6205	B2227+61	0.4431	124.6140	905.6	180	47	400$^\tau$

Table A.1. Pulsars not detected in this census. JName, BName: pulsar name. P0: pulsar period. DM: the DM used to coherently disperse the observations from Zakharenko et al. (2013) Stovall et al. (2015) and Bilous et al. (2016) and ATNF to complete. $\tau_{\text{scat}}^{\text{calc}}$/P0 : the scattering time (estimated using YMW16 Yao et al. (2017) at 60 MHz) divided by the pulsar period. duration: total duration of the observation in minutes. elev: the average elevation of the observation. upper limit for the mean flux: The upper limit for the mean flux density 1. $^\eta$: excluding the contribution of the nebula to T_{sky}. $^\tau$: upper limit for the mean flux density is not valid ($\tau_{\text{scat}}^{\text{calc}}$/P0$> 100$ %).
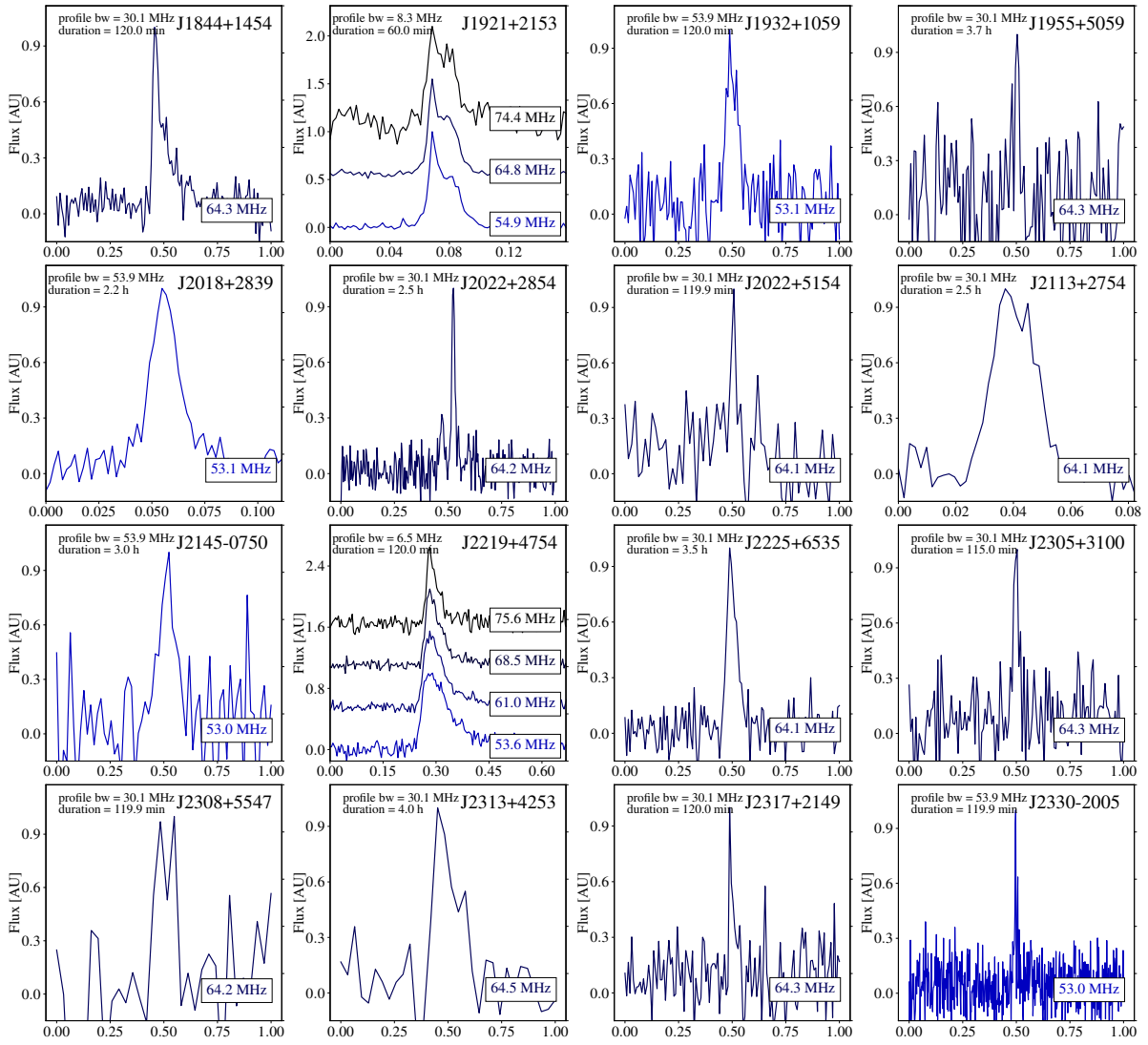
Appendix B: Pulsar profiles
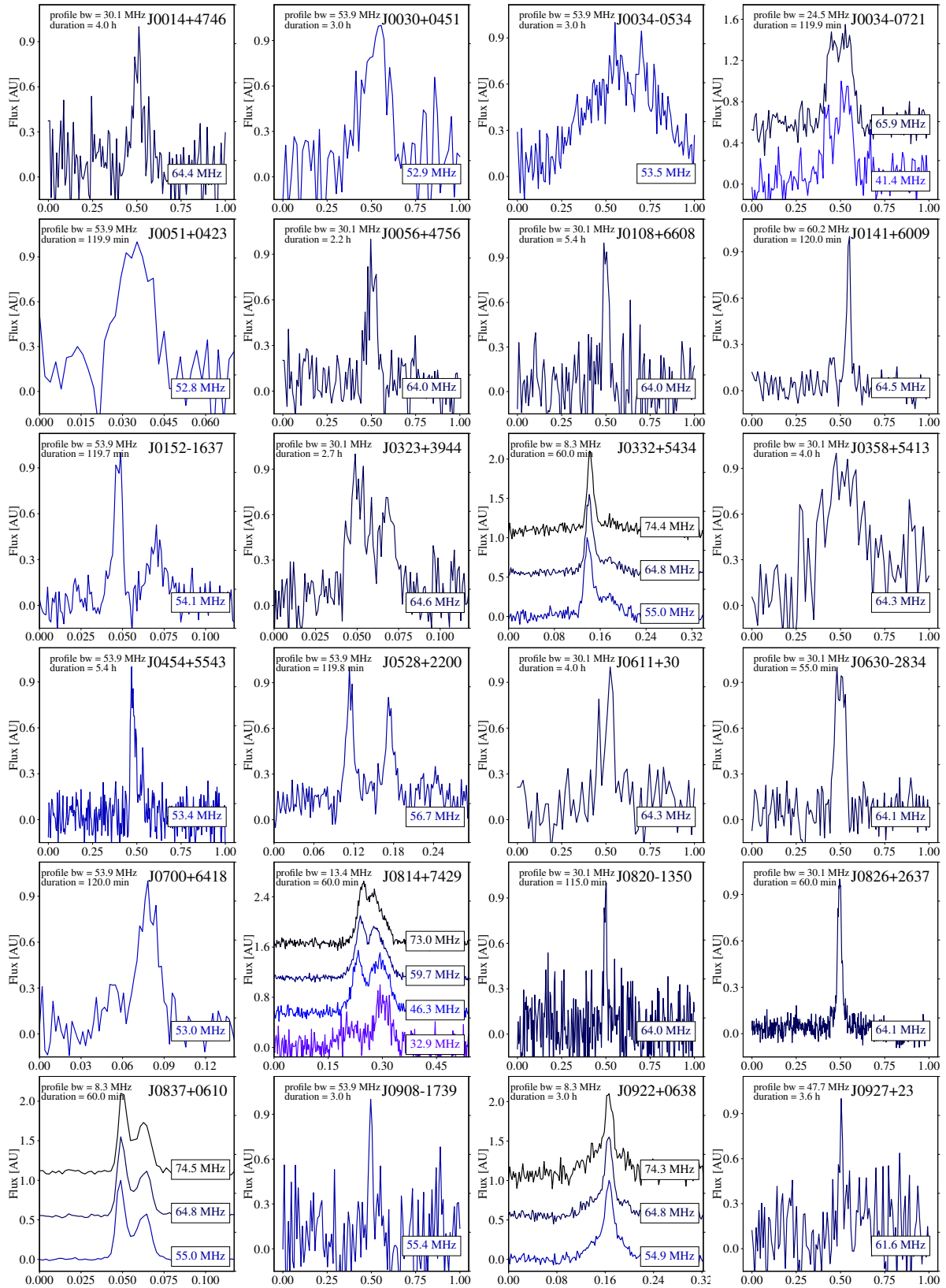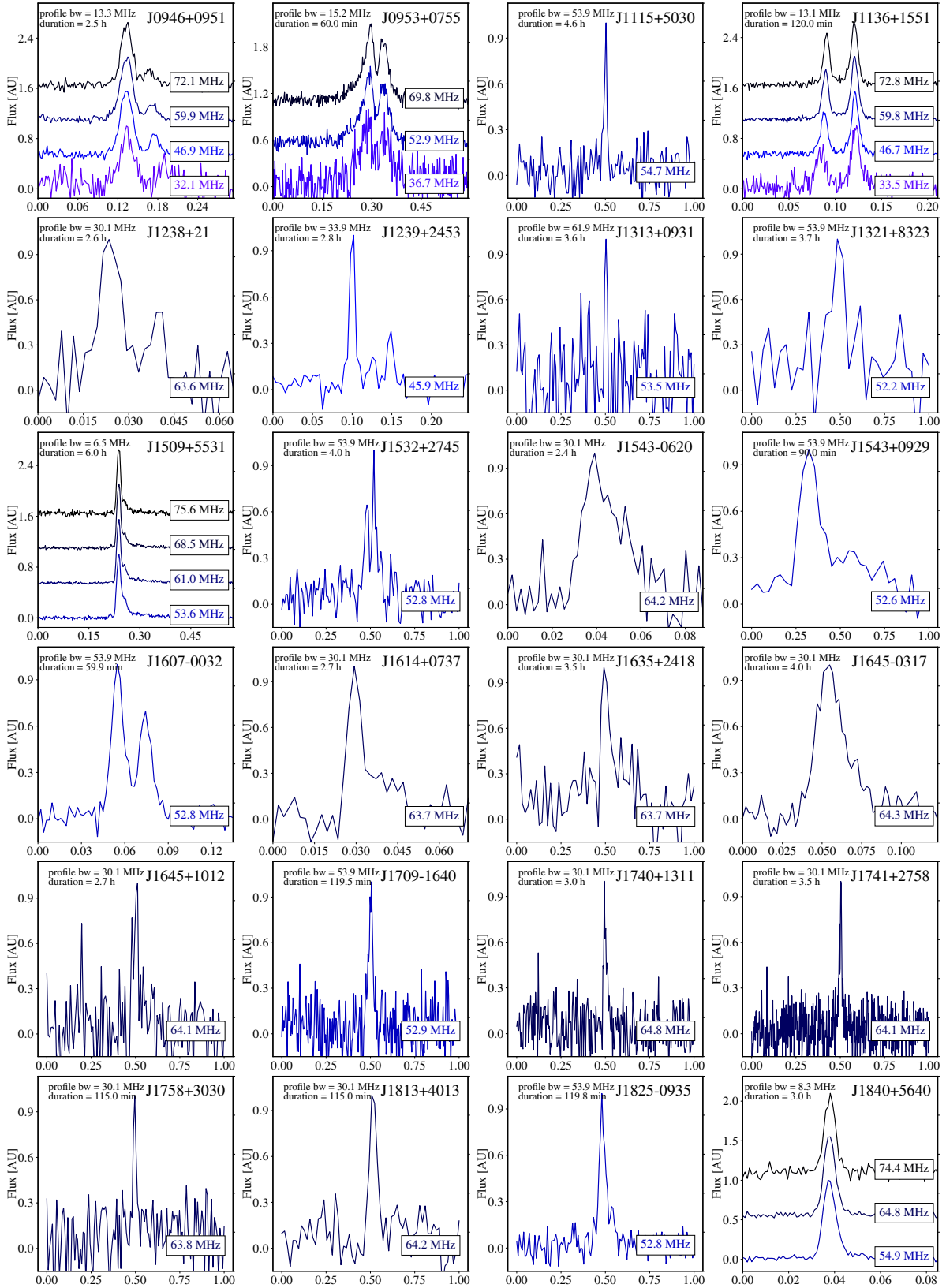
Fig. B.1. Profiles of the 64 pulsars detected in this work. The profiles are centered on the pulse region. Pulsars with a high signal-to-noise ratio are divided into several frequencies bands to show frequency dependent variations in the profiles. At the top left of each sub-figure, the bandwidth and the integration time used for each profile are indicated.